Dysfunctional Hippocampal-Prefrontal Connectivity without Neuronal Loss Is Associated with Psychotic-Like Behaviors Following Early-Life Seizure

Running head: HPC-PFC dysfunction and psychosis in epilepsy

Rafael Naime Ruggiero[1*], Danilo Benette Marques[1#], Matheus Teixeira Rossignoli[1#], Jana Batista De Ross[1], Tamiris Prizon[1], Ikaro Jesus Silva Beraldo[2,3], Lezio Soares Bueno-Junior[4], Ludmyla Kandratavicius[5], Jose Eduardo Peixoto-Santos[6], Cleiton Lopes Aguiar[2,3], João Pereira Leite[1*].

[1]Department of Neuroscience and Behavioral Sciences, Ribeirão Preto Medical School, University of São Paulo, Ribeirão Preto, São Paulo, Brazil.
[2]Department of Physiology and Biophysics Federal University of Minas Gerais, Belo Horizonte, Minas Gerais, Brazil.
[3]Laboratory of Molecular and Behavioral Neuroscience (LANEC), Federal University of Minas Gerais, Belo Horizonte, Brazil
[4]Department of Psychiatry, University of Michigan Medical School, Ann Arbor, Michigan, USA
[5]Department of Pathology, State University of Campinas, Campinas, São Paulo, Brazil
[6]Neuroscience Discipline, Department of Neurology and Neurosurgery, Universidade Federal de São Paulo, São Paulo, Brazil

***Corresponding author:** rafaruggiero@gmail.com, jpleite@fmrp.usp.br
[#]DBM and MTR contributed equally to this work

Conflict of interest

The authors declare no competing financial interests.

Acknowledgements

This research was funded by Fundação de Amparo à Pesquisa do Estado de São Paulo - FAPESP (R.N.R.: 2018/02303-4; M.T.R.: 2020/01510-6; J.P.L.:

2016/17882-4), Coordenação de Aperfeiçoamento de Pessoal de Nível Superior - CAPES - Finance Code 001 (D.B.M.: 88882.328283/2019-01;), and Conselho Nacional de Desenvolvimento Científico e Tecnológico - CNPq (J.P.L.: 305104/2020-9 and 422911/2021-6; T.P.: 164165/2018-5). We thank Renato Meirelles e Silva, Renata Caldo Scandiuzzi and Daniela Ribeiro for technical support. We thank Ana Carolina Medeiros and Rafael D'Agosta for helping with the photomicrography and histology. We also thank Patrick Forcelli, Claudio Queiroz, Marcelo Caetano, Tonicarlo Velasco, Ricardo Saute and Norberto Garcia Cairasco for discussions. RNR and JPL designed the research. RNR, CLA and LSBJ developed the methodology. RNR, DBM, TP and MTR conducted the experiments. RNR and DBM analyzed data. JBDR, LK, TP and JEPS performed immunohistochemistry. TP and JEPS conducted the neurochemistry experiments. JPL supervised the project. All authors wrote and revised the manuscript.

Abstract

Cognitive impairments and psychiatric symptoms affect up to half of temporal lobe epilepsy patients and are often more detrimental to their quality of life than the seizures themselves. Evidence indicates that the neurobiology of epileptogenesis shares common pathophysiological mechanisms with psychiatric comorbidities. However, these mechanisms and how they relate to specific behavioral alterations are unclear. We hypothesized that a dysfunctional communication between the hippocampus (HPC) and the prefrontal cortex (PFC), as a consequence of epileptogenesis, would be linked to behavioral and cognitive symptoms observed in the comorbidities of temporal lobe epilepsy. Here, we performed a multilevel study to investigate behavioral, electrophysiological, histopathological, and neurochemical long-term consequences of early-life *Status Epilepticus* in male rats. We found that adult animals submitted to early-life seizure (ELS) presented behavioral alterations typically found in animal models of psychosis, such as hyperlocomotion, reduction in sensorimotor gating, working memory deficits, and sensitivity to psychostimulants. Noteworthy, ELS rats did not exhibit neuronal loss. Instead, sensorimotor alterations were associated with increased neuroinflammation, as verified by glial fibrillary acidic protein (GFAP) expression, and altered dopamine

neurotransmission. Surprisingly, cognitive deficits were linked to an aberrant increase in HPC-PFC long-term potentiation (LTP). Furthermore, ELS rats displayed an abnormal brain state during active behavior characterized by oscillatory dynamics oddly similar to REM sleep. Our results point to impaired hippocampal-prefrontal network dynamics as a possible pathophysiological mechanism by which an epileptogenic insult can cause behavioral changes without neuronal loss. These convergent patterns of dysfunctional activity between epileptogenesis and psychosis bear translational implications for understanding psychiatric and cognitive comorbidities in epilepsy.

Introduction

Psychiatric disorders affect up to half of the patients with epilepsy and have a high impact on the quality of life. Understanding the neurobiological mechanisms of these comorbidities is crucial to develop better treatments for patients with epilepsy. It is currently speculated that the neurobiology of epileptogenesis shares common pathophysiological mechanisms with non-ictal symptoms, especially cognitive and psychiatric symptoms (Jensen, 2011). Temporal lobe epilepsy (TLE) is the most prevalent type of acquired epilepsy and presents a higher incidence of psychiatric comorbidities than the general population and other extratemporal epilepsies (Dalmagro et al., 2012). Patients with TLE frequently have a history of *Status Epilepticus* (SE) during infancy, which is seen as an initial injury that triggers epileptogenic processes (Mathern et al., 2002).

Experimental studies indicate that early-life seizures (ELS) induce long-term cognitive and behavioral alterations with translational validity for the psychiatric manifestations observed in clinical epilepsies (Holmes, 2016). However, ELS models are not associated with severe neuronal loss, unlike clinical or experimental TLE (Baram et al., 2002). One possible mechanism is that ELS could have effects at the brain circuit level, producing relevant cognitive impairments (Kandratavicius et al., 2012b, 2012a). The hippocampus (HPC) is a fundamental brain region affected by ELS and TLE. HPC interaction with the prefrontal cortex (PFC) underlies cognitive processes and is impaired in neuropsychiatric disorders such as schizophrenia (Ruggiero et al., 2021). Impairments of HPC-PFC oscillatory dynamics are observed in genetic,

developmental, and pharmacological models of schizophrenia and are thought to be essential to produce psychotic-like behavior (Sigurdsson, 2016).

Although it is well recognized that PFC and HPC are important for neuropsychiatric disorders, little is known about how their neuronal dynamics are affected after ELS. Here, we hypothesized that ELS would produce long-term alterations in HPC-PFC neuronal dynamics related to behavioral abnormalities and cognitive deficits (Ruggiero et al., 2012). To test this hypothesis, we induced ELS by SE and performed behavioral tests to assess sensorimotor and cognitive processes. Then, we performed neurophysiological, immunohistochemical, and neurochemical experiments to study potential changes in the HPC-PFC circuits that could underlie behavioral alterations. We found that adult ELS rats present behavioral impairments that are typically observed in animal models of psychosis and schizophrenia: hyperlocomotion, working memory deficits, sensorimotor gating impairment, and behavioral sensibility to psychostimulants. Remarkably, we found enhanced long-term potentiation (LTP) in HPC-PFC circuits, which was strongly associated with cognitive impairment. Our results also describe neuroinflammation and alterations in dopaminergic neurotransmission as major contributors to psychotic-relevant behavior. Furthermore, during active behavior, ELS rats displayed an aberrant brain state characterized by an oscillatory dynamic similar to REM sleep. Therefore, we identified a convergence of dysfunctional patterns at multiple levels linking epileptogenesis and psychotic-like behaviors. These convergent patterns indicate that epileptogenic processes triggered during early life, such as neuroinflammation, could lead to altered neurotransmission and consequently aberrant dynamics in the HPC-PFC coordination, potentially contributing to the psychiatric comorbidities of epilepsy.

Materials and Methods

Animals

Wistar rats were housed in a colony room with controlled temperature (22 ± 2 °C) and 12 h light/dark cycle with free access to food and water. Litters contained up to 8 animals with a maximum of 5 males. Rats were weaned at 21 days postnatally (P21). All procedures were performed according to the National Council for the Control of Animal Experimentation guidelines for animal research

and approved by the local Committee on Ethics in the Use of Animals (Ribeirão Preto Medical School, University of São Paulo; protocol: 159/2014).

Experimental Designs

We used four cohorts (total of 17 litters) to compare the effects of early-life *Status Epilepticus* (ELS) *versus* control (CTRL) animals. The first cohort was used for acute electrophysiology during the induction of ELS (n=5, ELS only). The second was used for behavioral tests (CTRL n=11, and ELS n=14), synaptic plasticity experiments (CTRL n=7, and ELS n=7), and immunohistochemistry (CTRL n=9, and ELS n=11). The third was used to investigate HPC-PFC dynamics in freely moving rats (CTRL n=6, and ELS n=9). Finally, in the fourth cohort we assessed behavioral sensitization to psychostimulants (CTRL n=15, and ELS n=14) and neurochemical quantification (CTRL n=8, and ELS n=9).

Early-Life Status Epilepticus

At P11-P12 we induced a 2-hour SE using lithium chloride (LiCl, 127 mg/kg, i.p., Sigma-Aldrich, USA) 18-20 prior to injection of methylscopolamine (1 mg/kg, i.p., Sigma-Aldrich) and pilocarpine (80 mg/kg, s.c., Sigma-Aldrich, USA) (Kubová and Mareš, 2013). SE was interrupted by diazepam (5 mg/kg, i.p., Teuto, Brasil) at the 2-hour mark. During the recovery period - 1 week post-ELS - food supplementation and subcutaneous rehydration with saline were provided. Body temperature and weight were monitored during the recovery period.

Behavior

The radial-arm maze - delayed non-match-to-sample task - was based on Floresco et al. (1997). Briefly, rats were kept at 85-90% of their initial body weight throughout the 21 days of the experiment. Training consisted of single daily sessions, each one divided into training phase and test phase, 30 minutes apart. During the training session, four doors were kept open providing access to food pellets. In the test session, all doors remained open, but with pellets available only in the four arms that were closed in the previous training session. The sessions were terminated upon full pellet consumption or after 5 min, whichever occurred first. Two types of errors were quantified. Reference error: reentering arms previously visited during the training session. Work error: reentering an arm

already visited during the test session. The sum of both categories denoted the total errors for each animal.

Animals were then examined for 30-min open field locomotion three days after the radial maze experiments to examine locomotion, with *ad libitum diet* (Wolf et al., 2016).

Immediately after the open field test, rats were examined for pre-pulse inhibition (PPI) of the acoustic startle. The PPI test consisted a habituation period (5 min) followed by 72 trials (intertrial interval: 15 ± 8 s) with pre-pulse alone (PP), startling pulse alone (P), pre-pulse followed by a startling pulse (PP + P), and no stimulus, all of which accompanied by a background noise (65 dB white noise). Startle-eliciting stimuli were presented at 120 dB for 40 ms (P) and prepulse stimuli were presented for 20 ms (PP, 1000 Hz; 71, 77, and 83 dB; 20 ms). Trials were presented in a random order, with each trial type being presented six times. We used the equation: %PPI = 100 − 100 × (mean startle amplitude at PP + P)/(mean startle amplitude at P) (Wolf et al., 2016).

In order to measure the effects of ELS on sensitization to psychostimulants we performed the apomorphine-induced locomotion test. At P80-90, rats were placed in the open field apparatus and allowed to roam for 60 minutes. We then injected apomorphine (APO, 1.5 mg/kg, i.p., Sigma-Aldrich, USA) and measured locomotion for another 60 min.

Synaptic Plasticity

HPC-PFC synaptic plasticity studies were performed as described in previous works from our group (Ruggiero et al., 2018; Lopes-Aguiar et al., 2020). Briefly, rats were anesthetized with urethane (1.2 mg/Kg in NaCl 0.15 M, i.p.) for electrode implantation. A recording electrode (Teflon-coated tungsten wires 60 µm, AM-Systems) was inserted in the medial PFC (Prelimbic region (PL), anterior-posterior: 3.0 mm; medial-lateral, ML: 0.5 mm; dorsal-ventral, DV: 3.2 mm), and a bipolar stimulation electrode (twisted wires; ~500 µm inter-pole distance) was inserted in the ipsilateral HPC (intermediate CA1 AP: −5.6 mm; ML: 4.5 mm; DV: 2.5 mm). An additional burr hole was drilled over the right parietal cortex for a reference screw. Temperature was kept constant at 37 ± 0.5°C during the experiment.

HPC was stimulated with single monophasic pulses (200 μs, 0.05 Hz, 150–300 μA, 80-ms inter-pulse interval) while recording PFC field postsynaptic potentials (fPSPs). Stimulation intensity (60–500 μA) was calibrated to evoke 50–60% of the maximal fPSP amplitude. Field recordings were conditioned through a preamplifier (100× gain, 0.03–3 kHz bandpass; Grass) and digitized at 10 kHz (ADInstruments). For LTP induction, we used a high-frequency stimulation (HFS) protocol consisting of 2 series (10 min apart) of 10 trains (0.1 Hz), each train with 50 pulses at 250 Hz (Ruggiero et al., 2018). fPSP amplitudes were computed as the difference between the positive and negative peaks. Short-term synaptic plasticity was estimated by paired-pulse facilitation (PPF), calculated as the ratio of the fPSP2 (Lopes-Aguiar et al., 2020) and fPSP1. Amplitudes were normalized as percentages of the baseline mean and averaged into 10 min bins.

Brain Tissue Processing

Immunohistochemistry

We employed a standardized immunohistochemistry protocol (Peixoto-Santos et al., 2015) to estimate NeuN+ neuronal density, to evaluate parvalbumin-expressing (PV) interneurons, glial fibrillary acid protein (GFAP) reaction, and mGluR5 expression. Briefly, endogenous peroxidases were blocked and the antigens were exposed by microwave-induced retrieval. We used the primary antibodies against NeuN (Chemicon, USA; 1:1000), PV (Calbiochem, USA; 1:500), mGluR5 (Millipore, USA; 1:200), and GFAP (Dako, Denmark; 1:500) proteins, and biotinylated secondary antibodies (Dako, Denmark; 1:200). Revelation was performed with Elite ABC Kit (Vector) and diaminobenzidine solution (Pierce).

Images from the regions of interest were captured at 200× magnification in Axio Scope.A1 microscope system (Carl Zeiss). The regions of interest included the hippocampus, entorhinal cortex (EC), infralimbic (IL) and prelimbic cortex (PL), and thalamic reticular nucleus (TRN). Images were then processed in Image J software (NIH, USA; 1.48v). Data are shown as the density of NeuN positive cells and immunopositive area for PV, mGluR5, and GFAP.

High-Performance Liquid Chromatography (HPLC)

Samples were taken bilaterally from the hippocampus, medial prefrontal neocortex, and nucleus accumbens (NAc). The samples were homogenized with ultrasound in a 0.1 mol/L $HClO_4$ 0.02% $Na_2S_2O_2$ solution containing dihydroxybenzylamine (DHBA, 146.5 ng/mL), and homoserine (HSER, 10 µg/mL) as internal standards and at a dilution of 15 µL per sample milligram. We employed Shimadzu LC-10AD isocratic systems with a fluorescence detector for glutamate (Glu) and gamma-aminobutyric acid (GABA), and an electrochemical detector for dopamine (DA), serotonin (5-HT) and their metabolites 3,4-dihydroxyphenylacetic acid (DOPAC) and 5-hydroxyindoleacetic acid (5-HIAA), as previously published (Castro-Neto et al., 2013). The neurotransmitter levels were considered to reflect neurotransmitter stock in synaptic vesicles, their metabolites reflected the release, and metabolite/neurotransmitter ratio were taken as an index of neurotransmitter turnover. Standards containing all amino acids and monoamines/metabolites of interest were employed to define their respective peaks in the samples.

Freely Moving Electrophysiology

Electrophysiological recordings

Chronic head caps consisted of two eight-channel connectors (Omnetics), one for the PFC (PL, 7 wires) and another for the HPC (intermediate CA1, 7 wires) (Marques et al., 2022). We additionally implanted a recording wire into the trapezius muscle for electromyogram (EMG). The EMG wire was soldered to the HPC connector. Microscrews were fastened into the skull, including a ground reference in the interparietal area. Animals were allowed to recover for 8-9 days before recordings.

To record electrophysiological signals through sleep-wake states, rats were placed into a shuttle box apparatus inside a soundproof box with food and water *ad libitum*. Recordings varied between 30 to 48 hours, divided later into periods of 6 hours for analysis. Local field potentials (LFP) were recorded through a multichannel acquisition processor (Plexon) (1000× gain, 0.7- to 500-Hz bandpass filter, 1-kHz sampling rate).

Classification of sleep-wake states

Classification of the sleep-wake cycle states was carried out through a semi-supervised machine-learning pipeline. The HPC theta (4.5-12 Hz), PFC delta (0.7-4 Hz), and EMG (100-200 Hz) power were computed in 5-second epochs without overlaps (4 tapers; time-bandwidth product: 2.5). A support vector machine (SVM) (radial basis function) was trained to discriminate the epochs into: (1) awake or sleep epochs using EMG power; (2) REM or NREM epochs based on theta/delta ratio; (3) quiet wake (QWK) or active (ACT) epochs based on theta/delta ratio. Later, we classified our recordings based on 30-second epochs by grouping sets of six 5-second epochs and considering the most representative state.

Spike-wave discharge (SWD) events were detected when the average short-time Fourier transform (STFT) power of the 4.4-16.4, 17.6-32.8, and 35.1-55 Hz frequency bands exceeded a certain threshold (mean + 1×standard deviation). Detected events were manually sorted by an expert.

Spectral estimates

We divided 30-s epochs into 3-s epochs for spectral analyses. Power spectrum densities (PSD) and magnitude-squared coherence were obtained using Welch's method with 1-s segments, 50% overlap, and Hamming windowing. Relative power was obtained by dividing values by the sum within 0.5-55 Hz for each epoch. To quantify theta oscillation we used the FOOOF algorithm (Donoghue et al., 2020), which parametrizes the PSD separating the periodic and aperiodic components of the signal. We used frequencies from 3 to 40 Hz, the ‘fixed’ aperiodic mode, minimum peak height of 0.05, and maximum number of peaks of 4 (https://fooof-tools.github.io/fooof/). EMG data were low-cut filtered (>30 Hz) and the sum of power within 30-200 Hz was obtained.

For power spectral correlations, we computed the spectrogram for each epoch using the STFT in a 100 ms Hamming window and 50 ms overlap, with signal padding to obtain a 0.5 Hz frequency bin from 0.5-200 Hz. We calculated the correlation matrix for each frequency pair using Pearson’s R.

Statemaps

After state classification and spectral analysis, we computed two-dimensional statemaps to investigate the natural distinction between sleep-wake

states. The statemaps were computed according to Gervasoni et al (2004) and Dzirasa et al (2006). First, we obtained the power *ratio 1* (4.5-9/4.5-50 Hz) and *ratio 2* (2-20/2-50 Hz) for each region and the first principal component, estimated by singular value decomposition algorithm considering both regions, for each ratio. Finally, we applied a Hann window of 10 epochs on scores throughout time for smoothing.

To identify the intermediate states (IS), we first estimated the trajectory *speed* of epochs throughout statemap dimensions as the Euclidean distance between each epoch and its predecessor. Then, we defined a threshold of 0.1 and labeled the epochs with greater speed as IS. This threshold was determined heuristically, corresponding closely to the expected value plus a standard deviation from a Poisson distribution across rats.

We used machine learning algorithms to decode sleep-wake states from the statemap. We used the ACT and REM statemap *ratio 1* and *2* values. We applied a linear and radial basis function SVM as well as a Random Forest algorithm using the *fitcensemble* function in MATLAB ('KernelFunction', 'linear' or 'rbf' for SVM, and 'Method', 'bag', 'NumLearningCycles', 500, for Random Forest) to decode states. We separated 20% of the epochs as test data. Discrimination was evaluated using the area under the receiver operating characteristic curve (AUC-ROC). Point-wise confidence interval was calculated using a 1000 repetition bootstrap.

Statistical Analysis

Data were analyzed using GraphPad Prism Software version 9.00 (GraphPad software, LLC), and R studio version 2021. We used paired Student *t*-tests for within-group comparisons and unpaired *t*-tests for between-group comparisons. Two-way ANOVA with repeated measures was performed for comparisons across time bins, using Sidak's Multiple Comparison Test as a post-hoc. To examine linear model assumptions, we analyzed the distribution of the residuals using a Q-Q plot, the Kolmogorov-Smirnov test, homoscedasticity and the residual plot. We used the Mann-Whitney test to compare two groups and the Wilcoxon signed-rank test to paired comparisons as non-parametric alternatives. We calculated Pearson linear correlation and Spearman's rank correlation as a nonparametric equivalent. To compare correlation and spectral coherence

estimates we applied Fisher's Z transform to the data. For multiple comparison in the neurochemical quantification, we performed Holm's procedure for multiple comparison correction across neurotransmitter/metabolite per region.

Data are expressed as the mean ± SEM. The significance level was set to 0.05 unless stated otherwise. Significances are expressed as $^{\dagger}p < 0.1$, $*p < 0.05$, $**p < 0.01$, and $***p < 0.001$.

Multivariate analysis

Data were Z-scored for each variable. Principal component analysis (PCA), using singular-value decomposition, was used for dimensionality reduction in order to find patterns of variance among multivariate behavioral and immunohistochemical data. Data were projected against principal components (PCs) and the mean score was compared between conditions.

Canonical correlation analysis (CCA) was performed to describe multivariate relationships between behavioral and neurobiological measures. Missing data were imputed using the MICE (Multiple Imputation by Chained Equations) algorithm. For CCA we used the psychotic and cognitive factor as input for the behavioral features and the PC1 of the NeuN, PV, GFAP and mGluR5 across all brain regions and the Z-scored LTP data as input for the neurobiological features. Using this approach, variables were narrowed down from 30 to 7, which is statistically appropriate for our sample size. We used the CCA package in R to obtain the canonical dimensions and performed the Wilks' Lambda, the Hotelling-Lawley Trace and a 1000 permutation resampling using Wilks' statistic to assess the significance of the dimensions.

We used multivariate generalized linear models (GLM) with a Gaussian family and an identity link function, using backward step-wise model selection based on Akaike Information Criteria. We used quasi-poisson regression (quasi-poisson family and logarithmic link function) for count data with overdispersion (Errors in the radial maze) using a quadratic covariate (LTP).

Results

ELS induces a psychotic-like behavioral phenotype

ELS induced by lithium-pilocarpine in early life (Fig. 1A) produced an unequivocal and stereotyped seizure, consisting mainly of forelimb myoclonus

and orofacial automatism (Racine 3) (Racine, 1971), with some animals showing further development into bilateral forelimb myoclonus, rearing and falling (Racine 4 and 5). Seizures were confirmed electrophysiologically, with paroxysms starting 10 min after pilocarpine injection and persisting for at least 120 min (Fig. 1B-C). Rats displayed weight loss on the day after ELS (Two-way RM ANOVA, treatment effect: $F_{(9,207)} = 11.7$, $p < 0.0001$, *post-hoc:* $p < 0.0001$; Fig. 1D,). However, ELS animals recovered the pace of normal weight gain in the subsequent days (*post-hoc*: $p > 0.05$) and into adulthood (Fig. 1E, unpaired *t*-test, $p > 0.05$), indicating that behavioral effects were unrelated to weight differences or alterations in food-seeking.

Next, we investigated the long-term behavioral consequences of ELS. ELS rats presented significantly higher locomotion in the open field test (Mann-Whitney test, $U = 27$, *n(CTRL, ELS)* = 11/14, $p = 0.0051$; Fig. 1F). ELS rats also presented a higher startle response (*t*-test, $t_{(23)} = 2.757$, $p = 0.011$; Fig. 1G) and a deficit in the sensorimotor gate represented by a reduction in pre-pulse inhibition (PPI) of the acoustic startle in all the three intensities tested (Two-way RM ANOVA, treatment effect: $F_{(2,46)} = 19.6$, $p < 0.0001$, *post-hoc:* PPI 71: $p = 0.0017$; PPI 77: $p = 0.0634$; PPI 83: $p = 0.030$; Fig. 1H,). Importantly, when examined for spatial memory, ELS rats presented a specific deficit in working memory errors (Mann-Whitney test, $U = 36.5$, *n(CTRL, ELS)* = 11, 14, $p = 0.0254$; Fig. 1I).

All these behavioral alterations are typical in animal models of psychosis (Sigurdsson, 2016). We investigated if collective patterns of behavioral alterations could reflect latent factors associated with these abnormalities. Working errors in the radial maze showed little correlation with the other behavioral variables while PPI intensities, startle response and locomotion in the open field were strongly correlated with each other (Fig. 1J). We also performed PCA to distinguish patterns of variance between multivariate behavioral data (Fig. 1K). Our analysis indicated that dimensionality reduction by PCA using two components explained more than 70% of the variability of the data (Fig. 1L). By analyzing the loadings of the two PCs, the variables that contribute more strongly (>0.5) to this dimension were: high total distance, startle reflex, and low PPI scores, indicating this component represents a latent factor of sensorimotor dysfunction related to psychotic-like behaviors. In turn, the PC2 represents the

cognitive dimension of the behavioral variables, as it presents a high loading value (>0.5) for working memory errors (Fig. 1M). Finally, we found that these PCs clearly distinguished CTRL from ELS animals, which presented higher values of PC1 and PC2 (*t*-test, $t_{(23)} = 3.9713$, $p = 0.0006$; Fig. 1N). These results indicate that the covariance of distinct behavioral tests can be represented by a latent *psychotic factor* (PC1) and a *cognitive factor* (PC2), representing two distinct dimensions of the behavioral phenotype.

Aberrant HPC-PFC synaptic plasticity in animals submitted to ELS

Next, we tested the hypothesis that behavioral abnormalities in ELS rats could be associated with impaired LTP of HPC-PFC circuits (Fig. 2A-C). First, we looked for ELS-related alterations in basal synaptic efficacy, prior to inducing LTP. Synaptic efficacy was assessed in terms of basal fPSP amplitude/slope, input-output curve (fPSP amplitude as a function of stimulus intensity) and PPF (fPSP amplitude as a function of inter-pulse interval). None of these measures indicated alterations in ELS when compared to CTRL (Fig. 2D-F).

We then proceeded to the actual synaptic plasticity experiments, and found that ELS rats presented an abnormally augmented LTP compared to CTRL (Fig. 2G-H; Two-way RM ANOVA, treatment effect: $F_{(1,12)} = 7.54$, $p = 0.0177$; interaction effect: $F_{(26,312)} = 7.393$, $p < 0.0001$; *post-hoc:* $p < 0.05$ for 10-60 min; *t*-test, $t_{(12)} = 2.747$, $p = 0.0177$; Fig. 2G inset), despite the lack of alterations in basal synaptic efficacy explained above (Fig. 2D-F). Aberrant LTP in the ELS rats was also observed when analyzing fPSP slope (Two-way RM ANOVA, treatment effect: $F_{(1,12)} = 4.757$, $p = 0.0498$; interaction effect: $F_{(26,312)} = 4.120$, $p < 0.0001$; *post-hoc:* $p < 0.05$ for 10-40 min; Fig. 2H; *t*-test, $t_{(23)} = 2.794$, $p = 0.0162$; Fig. 2H inset). Increased LTP was accompanied by a significant decrease in the PPF ratio during the initial 30 min of recording (Two-way RM ANOVA, interaction effect: $F_{(26,312)} = 3.457$, $p < 0.0001$; *post-hoc:* $p < 0.05$ for 20-30 min; Fig. 2I), possibly reflecting a ceiling effect on fPSP amplitude after LTP. With these results we demonstrate that ELS increases the ability of HPC-PFC circuits to undergo LTP, without changes to basal synaptic efficiency.

ELS induces long-term neural inflammation but not neuronal loss

We sought to investigate histopathological alterations that could underlie the behavioral abnormalities in the ELS rats (Fig. 3). Interestingly, ELS rats did not present neuronal loss when adults (Mann-Whitney test, $p > 0.05$; Fig. 3A). Since neuronal loss is a conspicuous finding related to cognitive deficits and behavioral alterations in clinical and experimental TLE, our data show that psychotic-like phenotypes can occur even without significant neuronal loss in the HPC or PFC. Also, ELS did not produce long-term effects in the expression of PV or mGluR5 receptors (Mann-Whitney test, $p > 0.05$; Fig. 3B-C). Finally, we investigated GFAP expression and observed a strong increase in neuroinflammation in ELS rats in all regions investigated except the infralimbic cortex (Mixed-effects model, $F_{(1,18)} = 5.368$, $p < 0.0325$; uncorrected Mann-Whitney test, $p < 0.05$ for granule layer (GL), CA1, EC, PL, and TRN; Fig. 3D). These results show that ELS produces brain inflammation later in life, but without an evident neuronal loss.

Neuroinflammation and abnormal LTP are distinctly correlated with psychotic-like behavior and cognitive impairment

Next, we conducted CCA to investigate the association between two groups of variables: the behavioral dimension and the neurobiological dimension, this latter combining the synaptic plasticity and immunohistochemical measures. By understanding the association between behavioral and neurobiological variables, we could infer putative mechanisms underlying the behavioral comorbidities observed in ELS animals. (Fig. 4A). CCA produced a significant high-correlation model ($r = 0.94$, Hotteling-Lawley Trace test, *F-approximation* $_{(10,12)} = 3.2311$, $p = 0.0164$ Fig. 4B) that clearly dissociated CTRL from ELS (behavioral canonical factor, *t*-test, $t_{(11)} = 3.693$, $p = 0.0035$; neurobiology canonical factor, *t*-test, $t_{(11)} = 3.917$, $p = 0.0024$; Fig. 4C). By analyzing the coefficients, we observed that the behavioral canonical dimension showed higher values for the psychotic factor, but also included the cognitive factor, although at a lower degree (Fig. 4D). The neurobiology canonical dimension showed a larger value for the GFAP, intermediate values for LTP and PV and low coefficients for NeuN and mGluR5 (Fig. 4D). A similar pattern was observed when analyzing the loadings for each dimension (Fig 4E). Taken together, these data suggest a strong correlation among the behavioral alterations produced by ELS, and a

strong correlation between the neurobiological variables GFAP and LTP. However, the neurobiological variables have only weak correlations between them (Fig. 4F).

We constructed multivariate generalized linear models (GLM) to further dissect the relationships between behavioral and neurobiological measures. The GLM indicates GFAP, PV, and LTP as the variables that most explain the behavioral variance (coefficients = 2.3775, 0.8457, and 0.5187; p = 0.1164, 0.00548, 0.08474 for GFAP, PV, and LTP, respectively Fig. 4G-H), with the increase in GFAP resulting in stronger behavioral abnormalities.

Strikingly, we found a quadratic relationship between synaptic plasticity effects and cognitive impairment. Poor performance on the working memory test was observed in rats that presented too low or too high values of HPC-PFC LTP, suggesting U-shaped relationships between LTP and cognitive performance (Fig. 4I). We observed this quadratic relationship using both PC2 (gaussian GLM, LTP coefficient = 1.22, p = 0.0162; Fig. 4I left) and raw error values from the radial maze test, using a quasi-Poisson GLM (Fig. 4I right).

Therefore, both neuroinflammation and synaptic plasticity alterations may underlie the behavioral effects of ELS, with neuroinflammation and LTP being more associated with the psychosis and cognition dimensions, respectively.

ELS animals present electrographical discharges when adults

Given the results above, we decided to further investigate the relationships between circuit and behavior dysfunctions using chronic electrophysiology. We classified LFP epochs into rapid eye movement sleep (REM), non-REM (NREM) sleep, quiet wake (QWK), and active wake (ACT, Fig. 5A-D). No ELS vs. CTRL differences were found in sleep architecture, according to mean consecutive duration, percentage of time awake, number of persistent episodes, or time spent in each state (Two-way RM ANOVA, $p > 0.05$; Fig. 5E-G).

We also examined if ELS animals presented ictal activity during recordings. We found that 44.45% of the ELS animals presented electrographic discharges similar to spike-wave discharges (SWD) or rhythmical spiking (Fig. 5H-I). SWDs occurred more often during NREM sleep and in the awake state, but rarely during REM (Fig 5J-L). The SWDs were not found in the CTRL rats, indicating that ELS induces an epileptogenic process.

Increased HPC theta is less coordinated with PFC gamma during behavioral activity in ELS **animals**

We then concentrated our investigation on the active wake state to look for associations between electrographic patterns and behavioral abnormalities. ELS rats presented higher theta power during active states in the HPC (Mann-Whitney, $U = 7$, $n(CTRL,$ ELS$) = 6/9$, $p = 0.0176$; Fig. 6A-C). Hippocampal theta is well known to occur during periods of locomotor activity, e.g., postural changes, head movements, and rearing. In this context, we can speculate that the further increase in theta power observed in ELS animals may be due to increased locomotion. To control for this, we co-examined theta power and EMG distributions during active states in ELS vs. CTRL (Fig. 6D). Theta oscillatory increase does not appear to be related to more movement, given that we do not observe a significant association between EMG and theta power. We found higher theta power even at low levels of EMG activity (Fig. 6D).

Finally, ELS animals showed a reduction in theta-gamma power correlation during active states (t-test, $t_{(13)} = 2.851$, $p = 0.0136$; Fig. 6E-G). Amplitude correlation is an indicator of large-scale cortical interactions that govern cognition (Siegel et al., 2012). Thus, Fig. 6E-G indicates that in ELS animals high-gamma activity is less correlated with theta power, which may in turn be related to the cognitive disruptions caused by ELS.

ELS rats display REM-like oscillatory dynamics during active behavior

To characterize long-term effects of ELS on HPC-PFC oscillatory dynamics across brain states, we constructed a statemap based on two spectral power ratios (Dzirasa et al., 2006; Gervasoni et al., 2004). This statemap framework allows consistent characterization of all major brain states, revealing a dynamic global structure produced by the collective activity of forebrain structures (Dzirasa et al., 2006). Thus, as expected, our statemaps presented three clearly distinct clusters corresponding to wake, REM, and NREM states (Fig. 7).

Surprisingly, however, ELS rats showed a significant overlapping between the REM and active states (Fig. 7A). We came to this conclusion by calculating the Euclidean distance between each REM and ACT epoch, and quantifying the

distributions of the Euclidean distances. While in CTRL rats the distributions were homogeneous and gaussian-shaped (Fig. 7B), ELS rats presented highly variable patterns across animals, some of which with skewed distributions (Fig. 7B). Indeed, the Euclidean distance was reduced in ELS vs. CTRL (t-test, t(13) = 2.326, p = 0.0369; Fig. 7D), suggesting that the spectral features of REM and active periods are more similar in ELS animals.

Interestingly, we observed that this statemap difference was stronger and more significant in the initial 12 hours of recording, which corresponds to the period when animals were habituating to the new environment (*t*-test, for Periods 1-2: $t_{(13)} = 2.45$, $p = 0.029$; for periods 3-4: $t_{(13)} = 0.9409$, $p = 0.3638$; Fig. 7E). To further verify the higher similarity between REM and active wake in ELS animals, we used machine learning (ML) algorithms as an attempt to separate these brain states through a brute-*force* approach. We observed that three ML algorithms had the worst discriminative performance in the ELS rats, represented by the lower AUC-ROC values (Fig. 7F). This lack of discriminative performance again indicated spectral similarities between REM and active state in ELS rats. These observations are consistent with a previous study (Dzirasa et al., 2006), which also described REM-like neural oscillations during novel environment exploration in animal models of hyperdopaminergia.

ELS rats present behavioral and neurochemical sensitivity to dopaminergic activation

We conducted a final experiment to investigate the susceptibility of ELS rats to dopaminergic activation using apomorphine (unspecific dopaminergic agonist). Our rationale was that previous studies reported REM-like neural oscillations during novel environment exploration in animal models of hyperdopaminergia (Dzirasa et al., 2006), which could have implications for the ELS alterations we described thus far. We examined behavioral sensitivity by comparing the locomotion produced by apomorphine in the open field (Fig. 8). Our data demonstrate that apomorphine produces a higher increase in locomotion in ELS rats when compared to CTRL across time-blocks (Two-way RM ANOVA, treatment effect: $F_{(1,27)} = 4.260$, $p = 0.0487$, *post-hoc:* 5 min $p = 0.0376$; Fig. 8A) or between average normalized distances (Mann-Whitney, *n(CTRL, ELS)* = 14/15, $U = 32$, $p = 0.0009$; Fig. 8A).

Immediately after finishing the behavioral test, rats were sacrificed to quantify neurotransmitters in HPC, PFC, and NAc. NAc was included in this analysis since NAc is highly implicated with dopamine sensitivity and exploratory behavior. Our data demonstrate that apomorphine reduces dopamine in the NAc of ELS rats, with no effects on dopamine turnover, as measured by DOPAC/DA ratio (Sidak's multiple correction procedure, $t_{(12)} = 3.656$, $p = 0.0033$; Fig. 8B-C). We also observed a reduction in dopamine turnover in the HPC of ELS rats (Sidak's multiple correction procedure, $U = 9$, $p = 0.0164$; Fig. 8D). A GLM model indicated that dopamine turnover in both NAc and HPC are significant predictors of apomorphine-induced hyperlocomotion (*coefficient* = -0.7108, $p = 0.00297$; Fig. 8C). Consistently, apomorphine is known to reduce endogenous DA release and DA metabolism in rodents and humans(Ozaki et al., 1989; de La Fuente-Fernández et al., 2001).

Regarding 5-HT quantification, we observed an increase in 5-HT content in NAc ($t_{(11)} = 5.053$, $p = 0.0004$; Fig. 8B), followed by a 5-HT turnover in both NAc and PFC (Sidak's multiple correction procedure, NAc: $U = 0$, $p = 0.0016$; PFC: $U = 8$, $p = 0.0104$; Fig. 8B, D). Interestingly, we found that the HPC of ELS rats shows a higher glutamate content and higher Glu/GABA ratio than CTRL animals following apomorphine injection (Sidak's multiple correction procedure, Glu: $t_{(15)} = 2.566$, $p = 0.0215$; Glu/GABA: $U = 9$, $p = 0.0079$; Fig. 8D).

Discussion

Here we showed that ELS leads to long-term behavioral abnormalities such as hyperlocomotion, poor sensorimotor gating, sensitivity to psychostimulants, and working memory deficits, which are well-established translational features of psychosis. Remarkably, these behaviors occurred independently of neuronal loss. Instead, they were correlated with neuronal inflammation, hypersensitive dopaminergic neurotransmission, and aberrant HPC-PFC synaptic plasticity. We also found that during active behavior ELS rats showed increased theta power with impaired coordination of local and long-range activity, in addition to abnormal oscillatory dynamics similar to REM sleep.

Common pathophysiological mechanisms underlying epileptogenesis, psychosis and cognitive impairments

Studies usually describe increased locomotion (Kubová and Mareš, 2013) and working memory deficits (Tsai et al., 2012) as consequences of ELS, consistent with our data. We also found reduced PPI, which is a less studied, but still well-established correlate of positive symptoms in clinical psychosis (Turetsky et al., 2007; Ziermans et al., 2011). Here we analyzed these behavioral abnormalities jointly, which resulted in a multivariate *behavioral factor* comprising multiple endophenotypes of psychosis reported in pharmacological, genetic, and developmental models of schizophrenia (Sigurdsson, 2016; Ruggiero et al., 2017). Thus, our study contributes a more holistic view of these co-occurring behavioral abnormalities. We were then able to dissect the behavioral factor into two uncorrelated components: psychotic and cognitive, and found that the latter was also impaired after ELS. This lack of association between behavioral and cognitive impairments suggests two neurobiological substrates, which are confirmed by our multivariate analysis, indicating the association of LTP to cognitive deficits and neuroinflammation to sensorimotor alterations.

More specifically, we found that cognitive impairments were associated with an abnormally increased susceptibility of HPC-PFC circuits to undergo LTP. This appears to be in contrast with previous studies, which reported reduced hippocampal LTP and cognitive deficits after ELS (Chang et al., 2003; O'Leary et al., 2016) However, no hyperexcitability or spontaneous seizures were described in these studies (O'Leary et al., 2016), which may explain their inconsistency with our data. Another study - Notenboom et al. (2010) - converged better with our data. Notenboom et al. (2010) used an animal model of prolonged febrile seizure at P10, and demonstrated increased LTP in HPC slices related to reduction of seizure threshold, hyperexcitability, and spontaneous seizures later in life (i.e., epileptogenesis) (Dube et al., 2000; Dubé et al., 2006). Indeed, prior to the studies above, paroxysmal activity had been shown to acutely increase synaptic efficacy and hippocampal LTP, thereby reducing the threshold for seizure induction (Ben-Ari and Gho, 1988; Minamiura A' et al., 1996). In this context, the enhanced LTP observed in our data indicates to a relationship with epileptogenesis, which concurs with the epileptiform discharges we observed in ~45% of our ELS rats, and the increases we observed in hippocampal glutamate/GABA ratio.

Here we also describe an inverted U-shaped relationship between LTP and working memory, suggesting that an optimal level of LTP susceptibility is required for adequate working memory performance. Aberrant synaptic plasticity could be a common mechanism between cognitive deficits and epileptogenesis. Hyperexcitable HPC-PFC circuits could facilitate the spread of epileptiform activity. This, in turn, could promote alterations in synaptic saturation and excitatory/inhibitory balance, ultimately leading to cognitive deficits. HPC-PFC synaptic plasticity is related to long-term memory storage, working memory capacity, and learning (Laroche et al., 2000; Ruggiero et al., 2021). It is hypothesized that both LTP and long-term depression in the HPC-PFC are critical for spatial learning, with these two forms of synaptic plasticity balancing each other to enhance or suppress information as needed (Laroche et al., 2000). In this sense, the abnormally increased LTP could impair sensory processes during working memory and explain the poor performance we observed in ELS rats. In a neural network with aberrantly enhanced LTP, synaptic plasticity could be biased toward potentiation, resulting in lower ability to retain information or adapt to the environment (Navakkode et al., 2022). This rationale is supported by several genetic studies, including on risk genes for neuropsychiatric disorders, that described relationships between enhanced LTP and impaired learning (Meng et al., 2002; Nuytens et al., 2013; Garcia-Alvarez et al., 2015; Yokoi et al., 2015; Navakkode et al., 2022). Also, enhanced LTP in HPC-PFC circuits is found in the methylazoxymethanol acetate (MAM) model of schizophrenia, which is also associated with impaired spatial working memory, reduced PPI, hypersensitivity to psychostimulants, and increased DA neurotransmission (Goto and Grace, 2006). In fact, administration of a D1 antagonist and a D2 agonist was shown to attenuate MAM-enhanced LTP (Goto and Grace, 2006), indicating that altered DA neurotransmission could underlie the LTP abnormalities we observed in ELS rats.

Here we also report an increase in GFAP expression in PFC, HPC, and thalamus in ELS animals. It is hypothesized in the literature that inflammatory processes initiated by epileptogenesis after a brain insult could lead to functional impairments and ultimately psychiatric symptoms (Vezzani et al., 2013). In ELS models, long-term glial activation has been related to behavioral impairments and epileptogenesis (de Oliveira et al., 2008), while treatment with inflammatory

inhibitors resulted in reductions of GFAP, cognitive impairments, and anxiety (Somera-Molina et al., 2007; Abraham et al., 2012). High levels of pro-inflammatory substances and neuroinflammation have been documented in both patients with schizophrenia and animal models of schizophrenia (Vezzani et al., 2013). Neural inflammation is also observed in psychiatric patients (Najjar et al., 2013) and epilepsy patients without psychiatric comorbidities (Kandratavicius et al., 2015). Noteworthy, the HPC of patients with TLE and interictal psychosis present greater GFAP and microglia activation compared to TLE patients with or without depression (Kandratavicius et al., 2015). These findings are in accordance with our multivariate analysis describing enhanced GFAP as the most important variable contributing to psychotic-like behavioral alterations in ELS animals.

In adult SE studies, behavioral abnormalities and cognitive deficits have been positively correlated to neuronal loss and spontaneous seizure frequency (Wolf et al., 2016), but this association cannot explain our findings. It is suggested that neuropsychiatric mechanisms and epileptic excitability spread progressively over time. Indeed, the behavioral impairments in ELS models tend to be more subtle than in animal models of TLE or psychosis. It is possible that the observed neuroinflammation, neuronal dynamics, and neurochemical alterations represent initial epileptogenic pathological mechanisms that could progress to spontaneous seizures, progressive neuronal loss, and more intense behavioral manifestations (Dube et al., 2000; Kubová and Mareš, 2013).

Dysfunctional patterns of HPC-PFC oscillatory dynamics

Our results demonstrate a locomotion-unrelated increase in HPC theta power during active behavior in ELS animals. Theta oscillations underlie various cognitive processes, including spatial memory and learning, and are believed to serve as a temporal organizer for multiple functions, such as sensorimotor integration (Buzsáki and Moser, 2013). However, increases in HPC theta power are also observed in altered psychotic-like states, such as following ketamine administration (Caixeta et al., 2013). Increases in theta power are also reported in most studies in patients with schizophrenia (Newson and Thiagarajan, 2019) and have been correlated with the poor cognitive performance of these patients (Curic et al., 2021). Thus, stronger HPC theta power does not necessarily reflect

an optimal cognitive state. In fact, here we observed lower theta-gamma correlations in the PFC of ELS animals, suggesting a disconnect between theta power and local coordination of PFC activity - which is reflected by gamma oscillations and thought to underlie cognitive processes. This could explain the cognitive-behavioral alterations we observed, at least to some extent.

Our results also demonstrated that during active behavior, frontal-limbic oscillatory dynamics of ELS rats are unusually similar to REM sleep. Importantly, we did not find alterations in locomotion or sleep architecture in ELS animals, suggesting that this REM-ACT similarity is highly specific to the frontal-limbic oscillatory dynamics we measured. This aberrant active state was maximal in the initial 12 h of recording, which corresponds to the period of habituation to the recording environment. Dzirasa et al (2006) found similar results when recording hyperdopaminergic mice. The authors described a REM-like awake state in DAT-KO mice and wild-type mice injected with amphetamine. Similar to our results, the hyperdopaminergic wake state was marked by a significant increase in hippocampal theta oscillations. Additionally, treatment with antipsychotics reduced these REM-like hippocampal oscillations (Dzirasa et al., 2006). This, in addition to our findings, suggests a common involvement of dopamine modulation in animal models of psychosis and epilepsy.

Apomorphine sensitivity has been associated with reduced PPI, hyperlocomotion, and increased NAc dopamine release (Ellenbroek and Cools, 2002). Corroborating our data, neonatal SE promotes amphetamine sensitization and affects both dopaminergic and glutamatergic prefrontal-striatal circuits (Lin et al., 2009). These results point to enhanced dopaminergic neurotransmission as a potential mechanism underlying the functional abnormalities observed in ELS rats.

In conclusion, we describe a comprehensive set of neurobiological and behavioral alterations following ELS, all of which reinforcing the relationship between epilepsy and psychosis. A prominent theory about the pathogenesis of schizophrenia links stressful insults during development to increased HPC excitability, which would culminate in the hyperactivation of the mesolimbic system, resulting in behavioral dysfunctions (Gomes et al., 2020). Our results add depth to this theory by finding relationships among: (1) epileptogenesis, (2) hyperexcitable HPC, (3) increased DA drive, (4) disrupted flow of information in

limbic-frontal circuits, and (5) psychosis-relevant behaviors. This multitude of mechanisms indicate how profound the long-term consequences of early-life seizures can be, and reinforce the importance of co-examining epilepsy and psychosis at several levels, from pathology to physiology and behavior.

References

Abraham J, Fox PD, Condello C, Bartolini A, Koh S (2012) Minocycline attenuates microglia activation and blocks the long-term epileptogenic effects of early-life seizures. Neurobiol Dis 46:425–430.

Baram TZ, Eghbal-Ahmadi M, Bender RA (2002) Is neuronal death required for seizure-induced epileptogenesis in the immature brain? In: Progress in Brain Research, pp 365–375. Elsevier.

Ben-Ari Y and, Gho M (1988) Long-lasting modification of the synaptic properties of rat ca3 hippocampal neurones induced by kainic acid.

Buzsáki G, Moser EI (2013) Memory, navigation and theta rhythm in the hippocampal-entorhinal system. Nat Neurosci 16:130–138.

Caixeta F v., Cornélio AM, Scheffer-Teixeira R, Ribeiro S, Tort ABL (2013) Ketamine alters oscillatory coupling in the hippocampus. Sci Rep. 3:2348.

Castro-Neto EF de, Cunha RH da, Silveira DX da, Yonamine M, Gouveia TLF, Cavalheiro EA, Amado D, Naffah-Mazzacoratti M da G (2013) Changes in aminoacidergic and monoaminergic neurotransmission in the hippocampus and amygdala of rats after ayahuasca ingestion. World J Biol Chem 4:141.

Chang Y-C, Huang A-M, Kuo Y-M, Wang S-T, Chang Y-Y, Huang C-C (2003) Febrile Seizures Impair Memory and cAMP Response-Element Binding Protein Activation. Ann Neurol. 2003 Dec;54(6):706-18.

Curic S, Andreou C, Nolte G, Steinmann S, Thiebes S, Polomac N, Haaf M, Rauh J, Leicht G, Mulert C (2021) Ketamine Alters Functional Gamma and Theta Resting-State Connectivity in Healthy Humans: Implications for Schizophrenia Treatment Targeting the Glutamate System. Front Psychiatry. 12:671007

Dalmagro CL, Velasco TR, Bianchin MM, Martins APP, Guarnieri R, Cescato MP, Carlotti CG, Assirati JA, Araújo D, Santos AC, Hallak JE, Sakamoto AC (2012) Psychiatric comorbidity in refractory focal epilepsy: A study of 490 patients. Epilepsy and Behavior 25:593–597.

de La Fuente-Fernández R, Lim AS, Sossi V, Holden JE, Calne DB, Ruth TJ, Stoessl AJ (2001) Apomorphine-Induced Changes in Synaptic Dopamine Levels: Positron Emission Tomography Evidence for Presynaptic Inhibition. J Cereb Blood Flow Metab. 21(10):1151-9.

de Oliveira DL, Fischer A, Jorge RS, da Silva MC, Leite M, Gonçalves CA, Quillfeldt JA, Souza DO, E Souza TM, Wofchuk S (2008) Effects of early-life LiCl-Pilocarpine-induced status epilepticus on memory and anxiety in adult rats are associated with mossy fiber sprouting and elevated CSF S100B protein. Epilepsia 49:842–852.

Donoghue T, Haller M, Peterson EJ, Varma P, Sebastian P, Gao R, Noto T, Lara AH, Wallis JD, Knight RT, Shestyuk A, Voytek B (2020) Parameterizing neural power spectra into periodic and aperiodic components. Nat Neurosci 23:1655–1665.

Dube C, Chen K, Eghbal-Ahmadi M, Brunson K, Soltesz I, Baram TZ (2000) Prolonged Febrile Seizures in the Immature Rat Model Enhance Hippocampal Excitability Long Term. Ann Neurol. 47(3):336-44.

Dubé C, Richichi C, Bender RA, Chung G, Litt B, Baram TZ (2006) Temporal lobe epilepsy after experimental prolonged febrile seizures: Prospective analysis. Brain 129:911–922.

Dzirasa K, Ribeiro S, Costa R, Santos LM, Lin SC, Grosmark A, Sotnikova TD, Gainetdinov RR, Caron MG, Nicolelis MAL (2006) Dopaminergic control of sleep-wake states. Journal of Neuroscience 26:10577–10589.

Ellenbroek BA, Cools AR (2002) Apomorphine Susceptibility and Animal Models for Psychopathology: Genes and Environment. Behav Genet. (5):349-61.

Floresco SB, Seamans JK, Phillips AG (1997) Selective Roles for Hippocampal, Prefrontal Cortical, and Ventral Striatal Circuits in Radial-Arm Maze Tasks With or Without a Delay. J Neurosci. 17(5):1880-90.

Garcia-Alvarez G, Shetty MS, Lu B, Yap KAF, Oh-Hora M, Sajikumar S, Bichler Z, Fivaz M (2015) Impaired spatial memory and enhanced long-term potentiation in mice with forebrain-specific ablation of the Stim genes. Front Behav Neurosci 9:180.

Gervasoni D, Lin SC, Ribeiro S, Soares ES, Pantoja J, Nicolelis MAL (2004) Global forebrain dynamics predict rat behavioral states and their transitions. Journal of Neuroscience 24:11137–11147.

Gomes F v., Zhu X, Grace AA (2020) Correction: The pathophysiological impact of stress on the dopamine system is dependent on the state of the critical period of vulnerability. Mol Psychiatry 25:3449.

Goto Y, Grace AA (2006) Alterations in Medial Prefrontal Cortical Activity and Plasticity in Rats with Disruption of Cortical Development. Biol Psychiatry 60:1259–1267.

Guyon N, Zacharias LR, de Oliveira EF, Kim H, Leite JP, Lopes-Aguiar C, Carlén M (2021) Network asynchrony underlying increased broadband gamma power. Journal of Neuroscience 41:2944–2963.

Holmes GL (2016) Effect of Seizures on the Developing Brain and Cognition. Semin Pediatr Neurol 23:120–126.

Jensen FE (2011) Epilepsy as a spectrum disorder: Implications from novel clinical and basic neuroscience. Epilepsia 52:1–6.

Jodo E, Suzuki Y, Katayama T, Hoshino KY, Takeuchi S, Niwa SI, Kayama Y (2005) Activation of medial prefrontal cortex by phencyclidine is mediated via a hippocampo-prefrontal pathway. Cerebral Cortex 15:663–669.

Kandratavicius L, Lopes-Aguiar C, Bueno-Júnior LS, Romcy-Pereira RN, Hallak JEC, Leite JP (2012a) Comorbidades psiquiátricas na epilepsia do lobo temporal: Possíveis relações entre desordens psicóticas e comprometimento de circuitos límbicos. Revista Brasileira de Psiquiatria 34:454–466.

Kandratavicius L, Peixoto-Santos JE, Monteiro MR, Scandiuzzi RC, Carlotti CG, Assirati JA, Hallak JE, Leite JP (2015) Mesial temporal lobe epilepsy with psychiatric comorbidities: A place for differential neuroinflammatory interplay. J Neuroinflammation 12:38.

Kandratavicius L, Ruggiero RN, Hallak JE, Garcia-Cairasco N, Leite JP (2012b) Pathophysiology of mood disorders in temporal lobe epilepsy. Revista Brasileira de Psiquiatria 34:233–259.

Kubová H, Mareš P (2013) Are morphologic and functional consequences of status epilepticus in infant rats progressive? Neuroscience 235:232–249.

Laroche S, Davis S, Se T, Jay M (2000) Plasticity at Hippocampal to Prefrontal Cortex Synapses: Dual Roles in Working Memory and Consolidation. Hippocampus. 10(4):438-46.

Lin TC, Huang LT, Huang YN, Chen GS, Wang JY (2009) Neonatal status epilepticus alters prefrontal-striatal circuitry and enhances methamphetamine-induced behavioral sensitization in adolescence. Epilepsy and Behavior 14:316–323.

Lopes-Aguiar C, Ruggiero RN, Rossignoli MT, Esteves I de M, Peixoto-Santos JE, Romcy-Pereira RN, Leite JP (2020) Long-term potentiation prevents ketamine-induced aberrant neurophysiological dynamics in the hippocampus-prefrontal cortex pathway in vivo. Sci Rep 10(1):7167.

Marques DB, Ruggiero RN, Bueno-Junior LS, Rossignoli MT, Leite JP (2022) Prediction of Learned Resistance or Helplessness by Hippocampal-Prefrontal Cortical Network Activity during Stress. Journal of Neuroscience 42:81–96.

Mathern GW, Adelson D, Cahan LD, Leite JR (2002) Hippocampal neuron damage in human epilepsy: Meyer's hypothesis revisited. Prog Brain Res135:237-51.

Meng Y, Zhang Y, Tregoubov V, Janus C, Cruz L, Jackson M, Lu W-Y, Macdonald JF, Wang JY, Falls DL, Jia Z (2002) Abnormal Spine Morphology and Enhanced LTP in LIMK-1 Knockout Mice. Neuron 35(1):121-33.

Minamiura A' Y, Hirayama K, Murata R, Matsuura S (1996) Effect of hyperthermia on hippocampal synaptic transmission and CA3 kindling in developing rats.

Najjar S, Pearlman DM, Alper K, Najjar A, Devinsky O (2013) Neuroinflammation and psychiatric illness. J Neuroinflammation 10:410:43.

Navakkode S, Zhai J, Wong YP, Li G, Soong TW (2022). Enhanced long-term potentiation and impaired learning in mice lacking alternative exon 33 of CaV1.2 calcium channel. Transl Psychiatry 12(1):1.

Newson JJ, Thiagarajan TC (2019) EEG Frequency Bands in Psychiatric Disorders: A Review of Resting State Studies. Front Hum Neurosci 12 :521.

Notenboom RGE, Ramakers GMJ, Kamal A, Spruijt BM, de Graan PNE (2010) Long-lasting modulation of synaptic plasticity in rat hippocampus after early-life complex febrile seizures. European Journal of Neuroscience 32:749–758.

Nuytens K, Gantois I, Stijnen P, Iscru E, Laeremans A, Serneels L, van Eylen L, Liebhaber SA, Devriendt K, Balschun D, Arckens L, Creemers JWM, D'Hooge R (2013) Haploinsufficiency of the autism candidate gene Neurobeachin induces autism-like behaviors and affects cellular and molecular processes of synaptic plasticity in mice. Neurobiol Dis 51:144–151.

O'Leary H, Bernard PB, Castano AM, Benke TA (2016) Enhanced long term potentiation and decreased AMPA receptor desensitization in the acute period following a single kainate induced early life seizure. Neurobiol Dis 87:134–144.

Ozaki N, Nakahara T, Miura H, Kasahara Y, Nagatsu S (1989) Effects of Apomorphine on In Vivo Release of Dopamine and Its Metabolites in the Prefrontal Cortex and the Striaturn, Studied by a Microdialysis Method. J Neurochem. 53(6):1861-4.

Peixoto-Santos JE, Velasco TR, Galvis-Alonso OY, Araujo D, Kandratavicius L, Assirati JA, Carlotti CG, Scandiuzzi RC, dos Santos AC, Leite JP (2015) Temporal lobe epilepsy patients with severe hippocampal neuron loss but normal hippocampal volume: Extracellular matrix molecules are important for the maintenance of hippocampal volume. Epilepsia 56:1562–1570.

Racine RJ (1971) Electroencephalography and Clinical Neurophysiology Modification of seizure activity by electrical stimulation: ii. Motor seizure. Electroencephalogr Clin Neurophysiol 32:281–294.

Ruggiero RN, Lopes-Aguiar C, Leite JP (2012) Early Life Seizures and Their Long-term Impacts on Cognition: The Role of Synaptic Plasticity Dysfunctions as an Underlying Mechanism. Journal of epilepsy and clinical neurophysiology 18:114-20.

Ruggiero RN, Rossignoli MT, de Ross JB, Hallak JEC, Leite JP, Bueno-Junior LS (2017) Cannabinoids and vanilloids in schizophrenia: Neurophysiological evidence and directions for basic research. Front Pharmacol 8:399.

Ruggiero RN, Rossignoli MT, Lopes-Aguiar C, Leite JP, Bueno-Junior LS, Romcy-Pereira RN (2018) Lithium modulates the muscarinic facilitation of synaptic plasticity and theta-gamma coupling in the hippocampal-prefrontal pathway. Exp Neurol 304:90–101.

Ruggiero RN, Rossignoli MT, Marques DB, de Sousa BM, Romcy-Pereira RN, Lopes-Aguiar C, Leite JP (2021) Neuromodulation of Hippocampal-Prefrontal Cortical

Synaptic Plasticity and Functional Connectivity: Implications for Neuropsychiatric Disorders. Front Cell Neurosci 15:732360.

Sigurdsson T (2016) Neural circuit dysfunction in schizophrenia: Insights from animal models. Neuroscience 321:42–65.

Somera-Molina KC, Robin B, Somera CA, Anderson C, Stine C, Koh S, Behanna HA, van Eldik LJ, Watterson DM, Wainwright MS (2007) Glial activation links early-life seizures and long-term neurologic dysfunction: Evidence using a small molecule inhibitor of proinflammatory cytokine upregulation. Epilepsia 48:1785–1800.

Tsai ML, Crutchley M, Boyce R, Ma J, Boon F, Cain DP, Leung LS (2012) Long-lasting auditory gating deficit accompanied by GABA B receptor dysfunction in the hippocampus after early-life limbic seizures in rats. Physiol Behav 106:534–541.

Turetsky BI, Calkins ME, Light GA, Olincy A, Radant AD, Swerdlow NR (2007) Neurophysiological endophenotypes of schizophrenia: The viability of selected candidate measures. Schizophr Bull 33:69–94.

Vezzani A, Aronica E, Mazarati A, Pittman QJ (2013) Epilepsy and brain inflammation. Exp Neurol 244:11–21.

Wolf DC, Bueno-Júnior LS, Lopes-Aguiar C, do Val Da Silva RA, Kandratavicius L, Leite JP (2016) The frequency of spontaneous seizures in rats correlates with alterations in sensorimotor gating, spatial working memory, and parvalbumin expression throughout limbic regions. Neuroscience 312:86–98.

Yokoi F, Chen HX, Dang MT, Cheetham CC, Campbell SL, Roper SN, Sweatt JD, Li Y (2015) Behavioral and electrophysiological characterization of Dyt1 heterozygous knockout mice. PLoS One 10(3):e0120916.

Ziermans T, Schothorst P, Magnée M, van Engeland H, Kemner C (2011) Reduced prepulse inhibition in adolescents at risk for psychosis: A 2-year follow-up study. Journal of Psychiatry and Neuroscience 36:127–134.

Figures and Legends

Figure 1. ELS induces a psychotic-like behavioral phenotype. ***A,*** Experimental design representing early-life SE induction and age of the animals during the experiments. ***B,*** Representative traces of LFP during baseline, motor seizure and ELS interruption (by injection of diazepam). ***C,*** Representative LFP from frontal cortex (top left) and HPC (top right) during baseline, ELS induction and ELS termination. LFPs are aligned with their respective spectrograms and energy curves on the bottom. ***D,*** Weight gain after ELS induction. ELS rats showed weight loss only on the ELS induction day. ***E,*** No weight differences between ELS and CTRL during experiments in adulthood, regardless if before food restriction (left) or during food

restriction (right). ***F,*** Higher locomotion of ELS rats in the open field test. ***G,*** higher acoustic startle of ELS rats. ***H,*** impaired sensory motor gating in ELS rats as measured using the PPI test with three stimulus intensities. ***I,*** *D*elayed non-match to sample (DNMTS) task on the radial maze. ELS rats showed a similar learning curve when compared to CTRL (right), and no differences were found in the number of reference errors (center). However, there was an increase in working memory errors across sessions. ***J,*** Correlation matrix of all behavioral variables. Note a cluster of positive correlations formed by the PPI measures, and another cluster of positive correlations formed by the distance traveled on the open field and the acoustic startle. These latter measures were negatively correlated with the PPI measures. Working memory errors were not correlated with the other behavioral features. ***K,*** Principal component analysis (PCA) of the behavioral features showing each animal projected onto the new factors. ***L,*** Explained variance from all principal components. ***M,*** Loadings of the behavioral variables on each principal component (PC) reveal a psychotic factor (PC1) and an uncorrelated cognitive factor (PC2). ***N,*** The psychotic factor distinguishes ELS from CTRL animals, as we compare the PC scores from each group. † $p < 0.1$, *$p < 0.05$, **$p < 0.01$, ***$p < 0.001$. Error bars represent the mean ± SEM.

Figure 2. Aberrant HPC-PFC synaptic plasticity in animals submitted to ELS. ***A,*** Experimental design including high-frequency stimulation (HFS). ***B,*** Electrode placement and representative electrolytic lesions in Nissl-stained coronal sections. ***C,*** Representative evoked fPSPs in the PFC. No difference between ELS and CTRL rats in terms of basal neurotransmission and synaptic efficacy, as shown by: ***D***, fPSP amplitude (left) and slope (right); ***E,*** input-output curve; and ***F,*** paired-pulse facilitation (PPF) curve. ***G,*** Despite no changes in basal synaptic efficacy, ELS rats showed aberrantly increased LTP, represented by higher fPSP amplitudes post-HFS, both across time blocks (main curve graph) and their averages (bar graph, inset). ***H,*** As in ***G,*** but from fPSP slopes. ***I,*** ELS rats showed reduced PPF in the initial 30 min (curve graph). Averaged data resulted in no differences between the groups (bar graph, inset). † $p < 0.1$, *$p < 0.05$, **$p < 0.01$, ***$p < 0.001$. Error bars represent the mean ± SEM.

Figure 3. ELS induces long-term neural inflammation, but not neuronal loss. Representative photomicrographs from immunohistochemistry each pair of columns represents a group comparison (left CTRL and right ELS) and each line is related to CA1 and PL, respectively. ***A,*** NeuN immunohistochemistry showing that ELS rats did not present neuronal loss. ***B,*** Parvalbumin (PV) immunohistochemistry. ***C,*** mGluR5: ***D***, GFAP, showing increased astrogliosis induced by early-life ELS. *$p < 0.05$ Error bars represent the mean ± SEM.

Figure 4. Neuroinflammation and abnormal LTP are distinctly correlated with psychotic-like behavior and cognitive impairment. ***A,*** Steps performed in data processing and analysis for canonical correlation analysis (CCA). ***B,*** CCA analysis showing CTRL and ELS animals projected onto the first canonical correlation. We found a strong correlation between the neurobiology canonical factor representing linear transformation of the neurobiological features and the behavior canonical factor representing the behavioral features. ***C,*** Canonical score showing the clear ELS vs. CTRL difference that the CCA was able to capture. ***D,*** Coefficients for behavior and neurobiology canonical factors, showing greater contribution of PC1, GFAP, PV and LTP for the correlation. ***E,*** Loadings of the behavioral and neurobiological variables on each canonical correlation dimension indicating association of GFAP and PV with the psychotic-like behavior. ***F,*** Correlation matrix representing only weak correlations between the neurobiological features. ***G,*** GLM regression between neurobiological features and the psychotic factor. ***H***, GLM model between neurobiological features and the psychotic factor show a strong association with GFAP, PV and LTP. ***I,*** GLM regression between LTP and the cognitive factor show a quadratic association (left). This quadratic association was further confirmed performing a quasi-Poisson regression between LTP and raw values of working memory errors (right). **$p < 0.01$. Error bars represent the mean ± SEM.

Figure 5. Classification of sleep-wake states and electrographic discharges in ELS rats. ***A,*** Electrode placement and representative electrolytic lesions in Nissl-stained coronal sections. ***B,*** Representative spectrogram, EMG RMS and theta/delta ratio used to score the sleep-wake cycle and to generate the hypnogram (bottom). ***C,*** Representative LFPs (top) recorded from PFC and HPC during ACT, NREM, REM and QWK. ***D,*** Average power spectral density for each state in the PFC and HPC of a representative animal. Note the increase in theta power during ACT and REM. ELS rats did not present alterations in the sleep-wake cycle. ***E,*** Mean duration of consecutive epochs for each state. No alterations in the ELS group. ***F,*** Percentage of time awake across 6-h blocks. No differences between ELS and CTRL animals. ***G,*** ELS caused no alterations in the number of persistent episodes (episodes lasting longer than 3 s, top) or the percentage of time spent in each state (bottom). ***H,*** Representative LFP from PFC and HPC showing a representative spike-wave discharge (SWD, top) and a poly-spike discharge (bottom). ***I,*** Electrographic discharges were found in 44.5% of ELS animals, and were absent in CTRL animals. ***J,*** Percentage of events occurring in each sleep-wake stage. ***K,*** Average total number of SWD events in CTRL and ELS animals. ***L,*** Frequency of SWDs occurring per state. SWDs events rarely occurred during REM. Error bars represent the mean ± SEM.

Figure 6. Increased HPC theta is less coordinated with PFC gamma during behavioral activity in ELS animals. ***A,*** Relative PSD of PFC during ACT. ***B,*** Relative PSD of HPC during ACT. ***C,*** ELS rats presented enhanced HPC theta power during ACT, according to a parametric model that distinguishes oscillatory from aperiodic components. ***D,*** Theta power increase in ELS rats was unrelated to locomotor activity. Distributions of relative theta power and Z-scored EMG values for all rats. EMG power was not related to the regions of greater theta power in ELS animals. ***E*** Grand-average amplitude correlogram for CTRL (left) and ELS (right) group. Note the absence of amplitude correlation between theta and gamma activity in the ELS group. ***F,*** High-gamma (65-100 Hz) correlation with low frequency activity. Note the peak around theta oscillation in the CTRL group, which was absent in ELS. ***G,*** ELS animals presented impaired theta-gamma amplitude correlation. † $p < 0.1$, *$p < 0.05$. Error bars represent the mean ± SEM.

Figure 7. ELS rats display REM-like oscillatory dynamics during active behavior. ***A,*** Representative statemaps from three CTRL (top) and three ELS (bottom) rats. CTRL rats displayed a clear separation between REM (red), ACT (green) and NREM (blue) clusters. ELS displayed an overlap between REM and ACT states. ***B,*** Distributions of the Euclidean distances between each REM and ACT epoch for CTRL (top) and ELS (bottom) rats. ELS distributions were heterogeneous, some of which were skewed. ***D,*** Average Euclidean distance showing that ELS rats have a REM-like oscillatory dynamics during active behavior. ***E,*** The REM-like oscillations during ACT were higher during the initial 12 h of recording. ***F,*** Machine learning approach to decode REM *versus* ACT states. We used linear SVM, radial basis function SVM and random forest (RF) algorithm in order to classify REM and ACT epochs in CTRL (black) or ELS (red) rats. Using a bootstrapped confidence interval, we observed that the discriminative performance was worse in ELS animals, even when using “brute-force” algorithms. † $p < 0.1$, *$p < 0.05$, **$p < 0.01$, ***$p < 0.001$. Error bars represent the mean ± SEM.

Figure 8. ELS rats present behavioral and neurochemical sensitivity to dopaminergic activation. ***A,*** Normalized locomotion across time blocks after apomorphine (APO) injection, demonstrating increased locomotion of ELS rats after APO injection. Average normalized locomotion after APO injection (inset). ***B,*** Concentration of dopamine and metabolites (upper panel) and 5-HT and metabolites (lower panel) in the NAc. ***C,*** GLM for the total distance after APO indicating DOPAC/DA ratio in the NAc as a strong significant variable associated with behavioral sensibility to APO. ***D,*** Concentration of dopamine and metabolites (left), 5-HT and metabolites (center) and glutamate and GABA (right) in the PFC (upper panel) and HPC (lower panel). †Uncorrected $p < 0.05$, * multiple comparison corrected $p < 0.05$. Error bars represent the mean ± SEM.

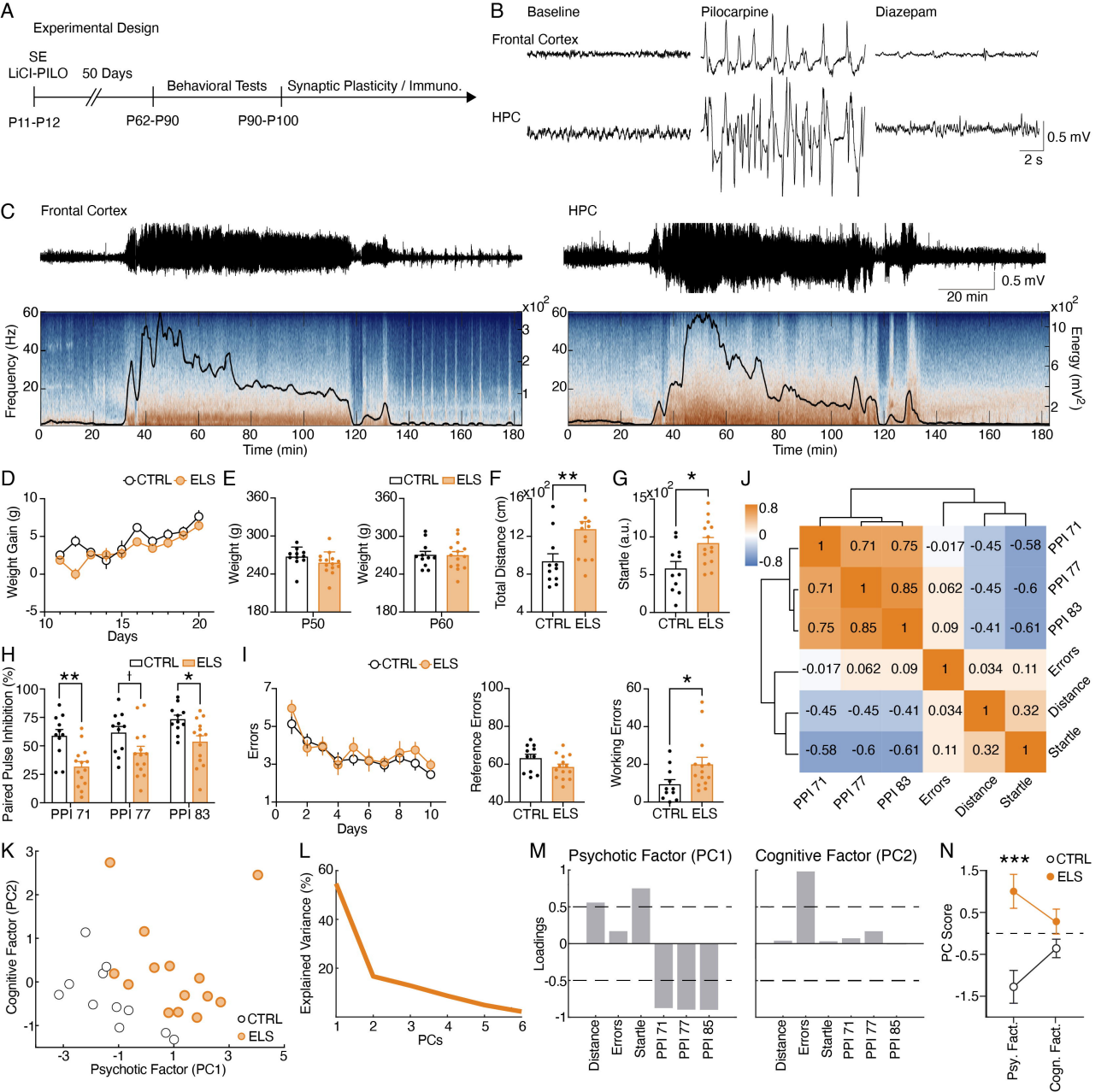
A
Experimental Design
SE
LiCl-PILO
50 Days
Behavioral Tests
Synaptic Plasticity / Immuno.
P11-P12
P62-P90
P90-P100
B
Baseline
Pilocarpine
Diazepam
Frontal Cortex
HPC
0.5 mV
2 s
C
Frontal Cortex
HPC
0.5 mV
20 min
Frequency (Hz)
Energy (mV²)
Time (min)
D
CTRL
ELS
Weight Gain (g)
Days
E
Weight (g)
P50
P60
F
Total Distance (cm)
CTRL
ELS
G
Startle (a.u.)
J
PPI 71
PPI 77
PPI 83
Errors
Distance
Startle
H
Paired Pulse Inhibition (%)
PPI 71
PPI 77
PPI 83
I
Errors
Days
Reference Errors
Working Errors
K
Cognitive Factor (PC2)
Psychotic Factor (PC1)
L
Explained Variance (%)
PCs
M
Psychotic Factor (PC1)
Cognitive Factor (PC2)
Loadings
Distance
Errors
Startle
PPI 71
PPI 77
PPI 85
N
PC Score
Psy. Fact.
Cogn. Fact.

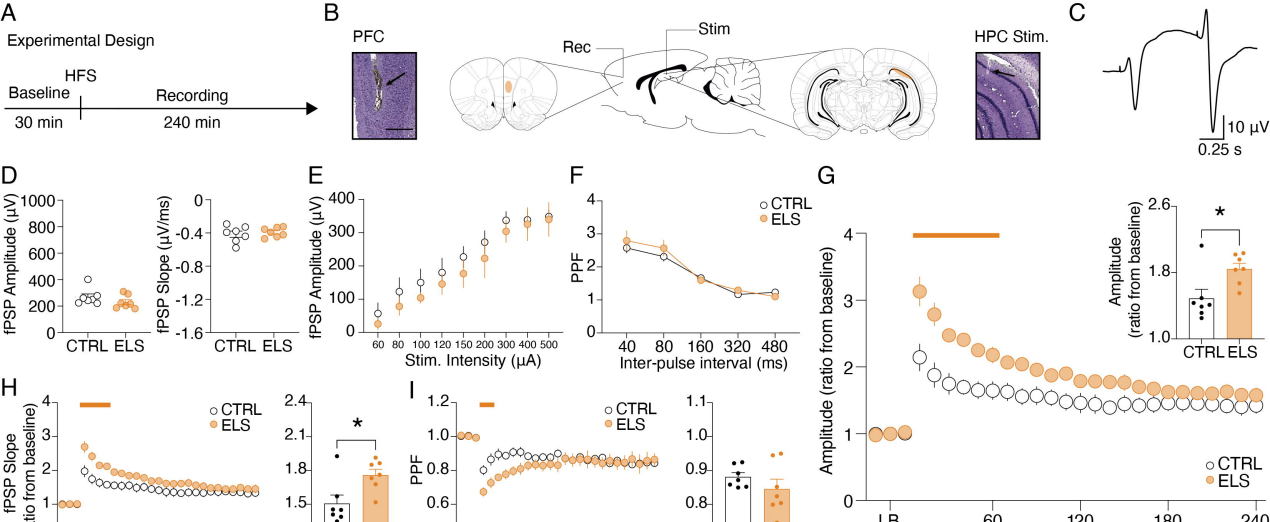
A
Experimental Design
HFS
Baseline
Recording
30 min
240 min
B
PFC
Rec
Stim
HPC Stim.
C
10 μV
0.25 s
D
fPSP Amplitude (μV)
fPSP Slope (μV/ms)
CTRL ELS
E
fPSP Amplitude (μV)
Stim. Intensity (μA)
F
PPF
Inter-pulse interval (ms)
CTRL
ELS
G
Amplitude (ratio from baseline)
Time (min)
LB
H
fPSP Slope (ratio from baseline)
Time (min)
I
PPF
Time (min)

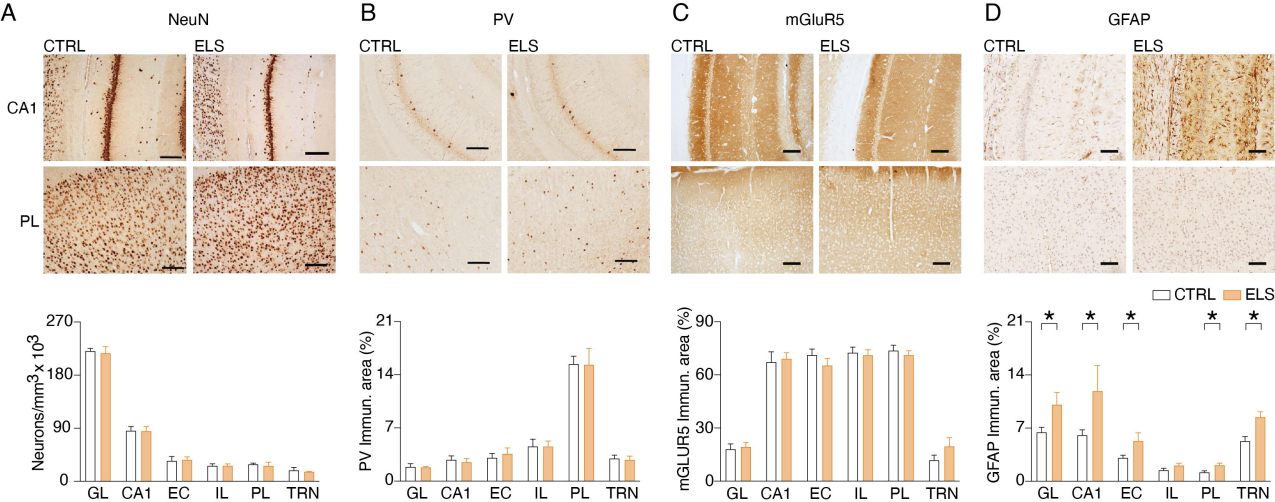
A
NeuN
CTRL
ELS
CA1
PL
B
PV
C
mGluR5
D
GFAP
CTRL
ELS
Neurons/mm3 x 10^3
270
180
90
0
GL
CA1
EC
IL
PL
TRN
PV Immun. area (%)
21
14
7
mGLUR5 Immun. area (%)
90
60
30
GFAP Immun. area (%)
*

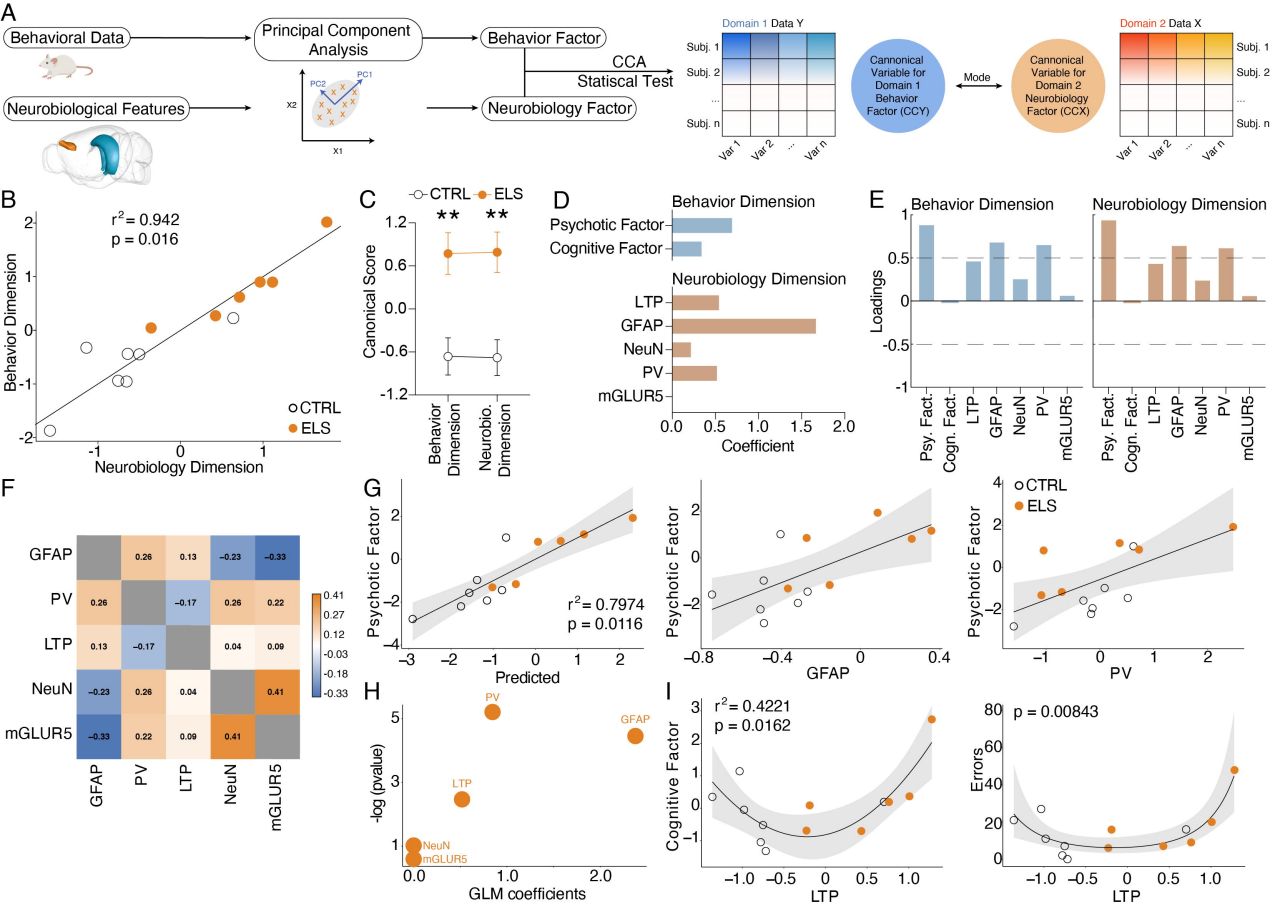
A
Behavioral Data
Principal Component Analysis
Behavior Factor
Neurobiological Features
Neurobiology Factor
CCA
Statiscal Test
PC2
PC1
X2
X1
Domain 1 Data Y
Subj. 1
Subj. 2
Subj. n
Var 1
Var 2
Var n
Cannonical Variable for Domain 1 Behavior Factor (CCY)
Mode
Cannonical Variable for Domain 2 Neurobiology Factor (CCX)
Domain 2 Data X
B
r2 = 0.942
p = 0.016
Behavior Dimension
Neurobiology Dimension
CTRL
ELS
C
CTRL
ELS
Canonical Score
Behavior Dimension
Neurobio. Dimension
D
Behavior Dimension
Psychotic Factor
Cognitive Factor
Neurobiology Dimension
LTP
GFAP
NeuN
PV
mGLUR5
Coefficient
E
Behavior Dimension
Neurobiology Dimension
Loadings
Psy. Fact.
Cogn. Fact.
LTP
GFAP
NeuN
PV
mGLUR5
F
GFAP
PV
LTP
NeuN
mGLUR5
G
Psychotic Factor
Predicted
r2 = 0.7974
p = 0.0116
GFAP
PV
CTRL
ELS
H
-log (pvalue)
GLM coefficients
PV
GFAP
LTP
NeuN
mGLUR5
I
Cognitive Factor
LTP
r2 = 0.4221
p = 0.0162
Errors
p = 0.00843

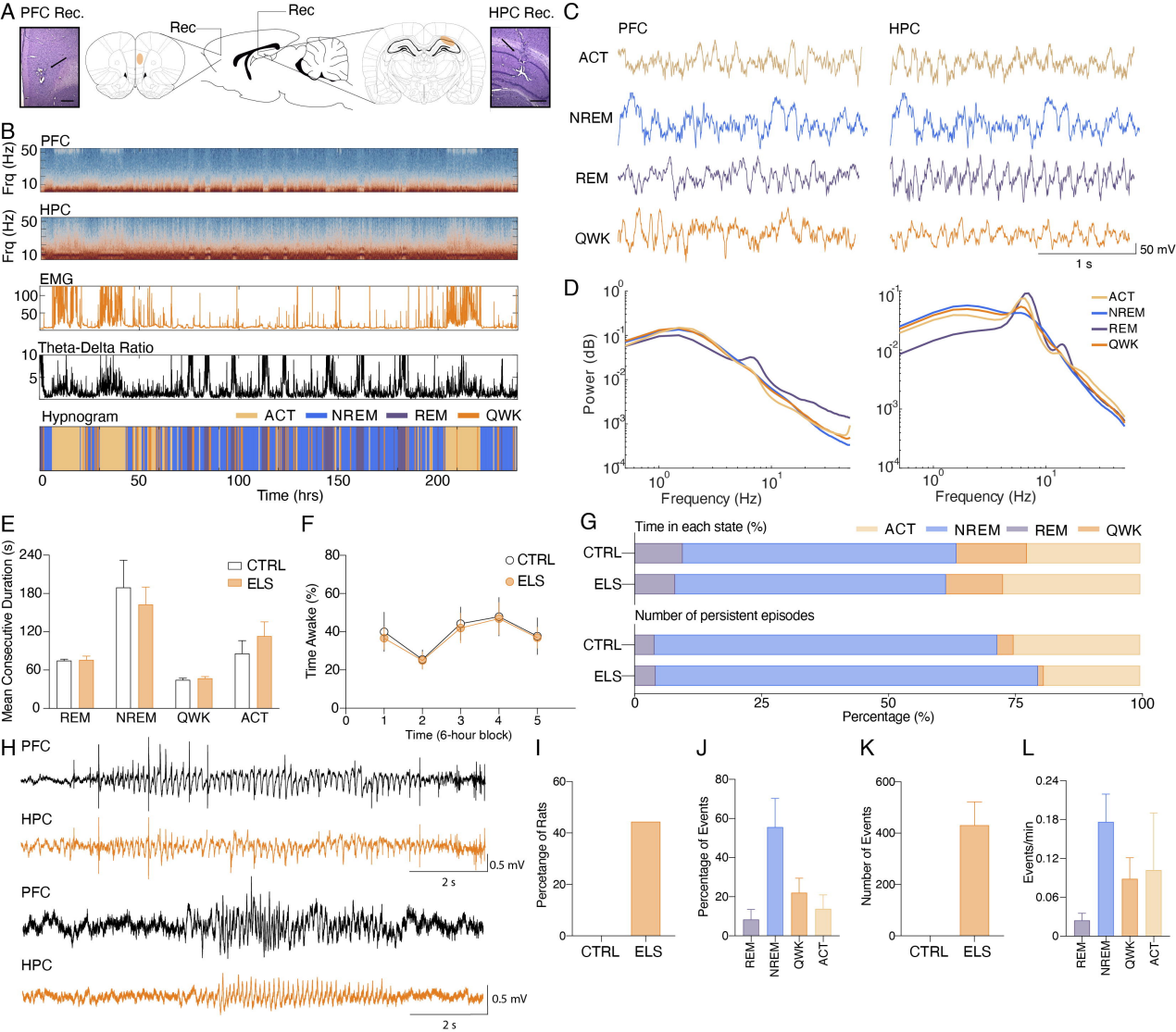
A
PFC Rec.
Rec
Rec
HPC Rec.
B
PFC
Frq (Hz)
50
10
HPC
Frq (Hz)
50
10
EMG
100
50
Theta-Delta Ratio
10
5
Hypnogram
ACT
NREM
REM
QWK
0
50
100
150
200
Time (hrs)
C
PFC
HPC
ACT
NREM
REM
QWK
1 s
50 mV
D
Power (dB)
Frequency (Hz)
Frequency (Hz)
ACT
NREM
REM
QWK
E
Mean Consecutive Duration (s)
240
180
120
60
0
CTRL
ELS
REM
NREM
QWK
ACT
F
Time Awake (%)
80
60
40
20
0
CTRL
ELS
0
1
2
3
4
5
Time (6-hour block)
G
Time in each state (%)
ACT
NREM
REM
QWK
CTRL
ELS
Number of persistent episodes
CTRL
ELS
0
25
50
75
100
Percentage (%)
H
PFC
HPC
0.5 mV
2 s
PFC
HPC
0.5 mV
2 s
I
Percetange of Rats
60
40
20
0
CTRL
ELS
J
Percentage of Events
80
60
40
20
0
REM
NREM
QWK
ACT
K
Number of Events
600
400
200
0
CTRL
ELS
L
Events/min
0.24
0.18
0.12
0.06
0
REM
NREM
QWK
ACT

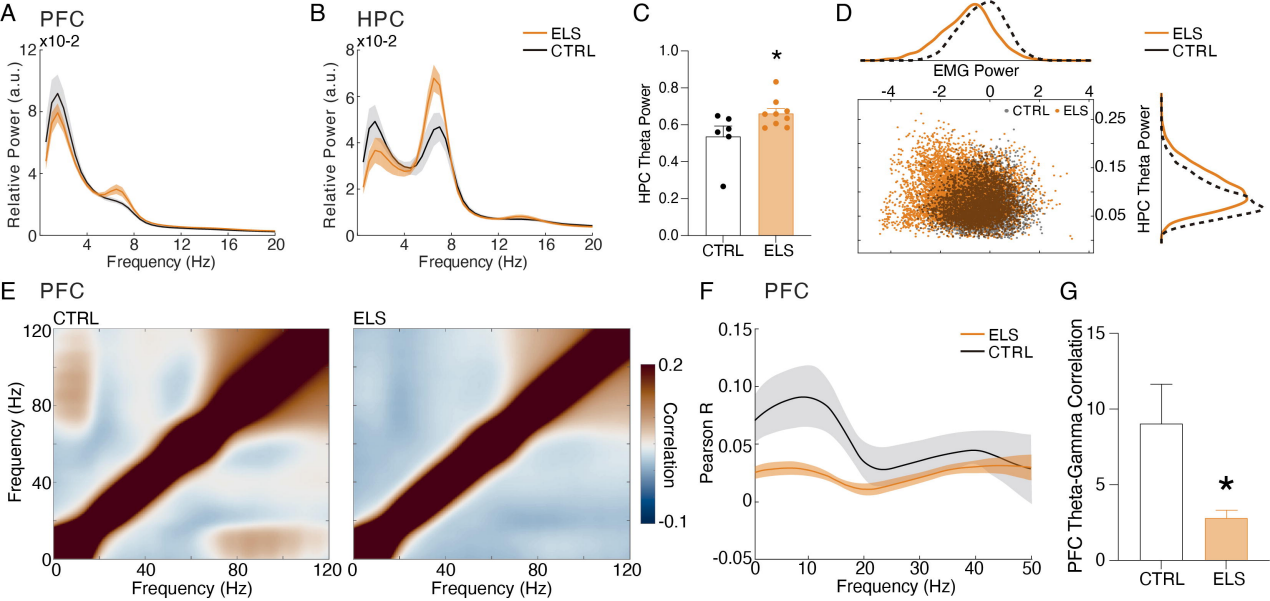
A
PFC
x10-2
Relative Power (a.u.)
Frequency (Hz)
B
HPC
ELS
CTRL
C
HPC Theta Power
CTRL
ELS
D
EMG Power
HPC Theta Power
E
PFC
CTRL
ELS
Frequency (Hz)
Correlation
F
PFC
Pearson R
G
PFC Theta-Gamma Correlation

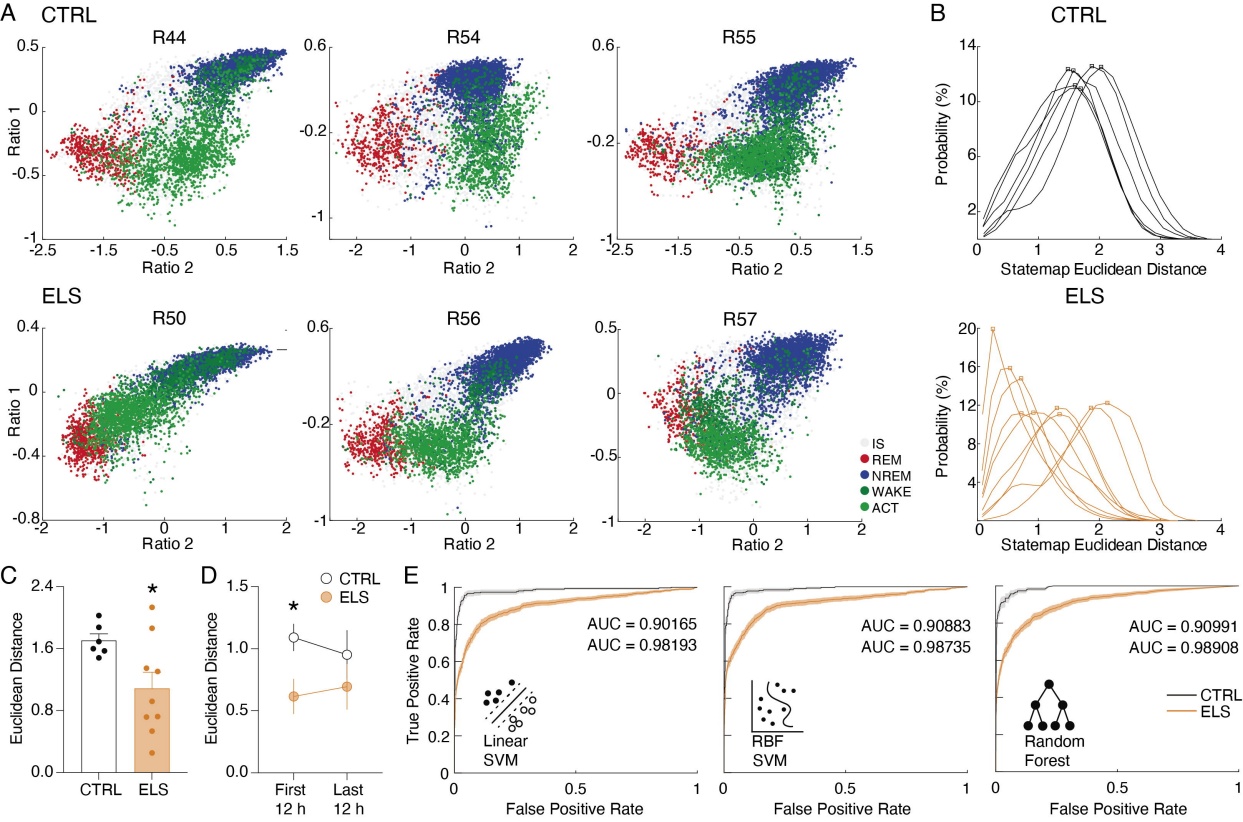
A
CTRL
R44
R54
R55
Ratio 1
Ratio 2
ELS
R50
R56
R57
IS
REM
NREM
WAKE
ACT
B
CTRL
ELS
Probability (%)
Statemap Euclidean Distance
C
Euclidean Distance
CTRL
ELS
D
CTRL
ELS
First 12 h
Last 12 h
E
True Positive Rate
False Positive Rate
AUC = 0.90165
AUC = 0.98193
Linear SVM
AUC = 0.90883
AUC = 0.98735
RBF SVM
AUC = 0.90991
AUC = 0.98908
Random Forest
CTRL
ELS

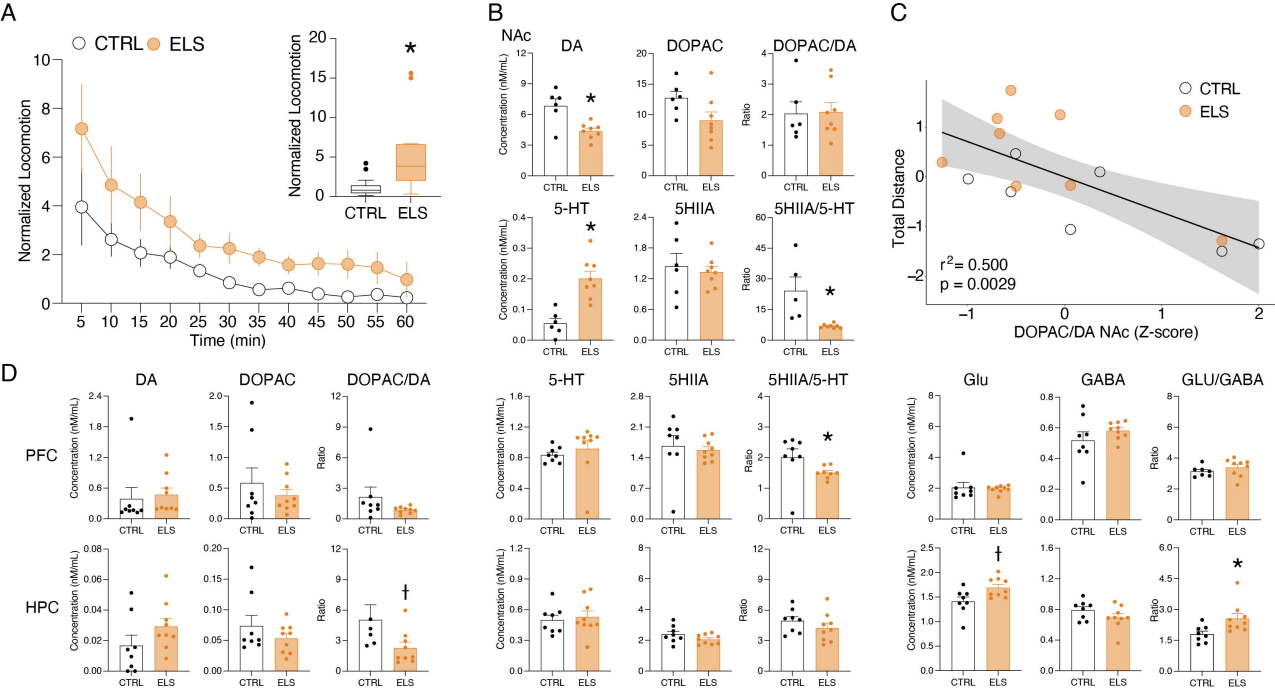
A
CTRL
ELS
Normalized Locomotion
Time (min)
Normalized Locomotion
CTRL
ELS
B
NAc
DA
DOPAC
DOPAC/DA
5-HT
5HIIA
5HIIA/5-HT
Concentration (nM/mL)
Ratio
C
CTRL
ELS
Total Distance
DOPAC/DA NAc (Z-score)
r2= 0.500
p = 0.0029
D
PFC
HPC
DA
DOPAC
DOPAC/DA
5-HT
5HIIA
5HIIA/5-HT
Glu
GABA
GLU/GABA
Concentration (nM/mL)
Ratio